JOURNAL OF MATERIALS SCIENCE 17 (1982) 3575–3592

The formation and properties of mineral–polyacid cements

Part 2 *Chain, sheet and three-dimensional silicates*

PETER R. HORNSBY
Department of Non-Metallic Materials, Brunel University, Uxbridge, Middlesex, UK
SHEILA A. MERSON, HAVARD J. PROSSER, ALAN D. WILSON
Laboratory of the Government Chemist, Cornwall House, Stamford Street, London SE1, UK

The cement-forming characteristics of selected chain, sheet and framework silicates when mixed with aqueous solutions of acrylic acid polymers have been investigated using infrared spectroscopy, X-ray diffraction, chemical analysis and the measurement of physical properties. The initial stages of the cement-forming reaction were investigated by measuring the release of elements from minerals into acid solution and estimating the extent of mineral decomposition. The degree of neutralization and the structure of the polysalt matrix were determined by infrared spectroscopy.

1. Introduction

The need for improved dental cements has stimulated the development of a new class of material, generally termed an ionic polymer cement. Although a wide variety of ion-leachable inorganic powders and aqueous polyacid solutions will react together yielding products of this type, many have limited strength, are unstable to water and consequently have little practical value [1–3]. However, when modified zinc oxide powders or specially formulated calcium aluminosilicate glass powders are combined with aqueous solutions of poly(alkenoic acids), such as poly(acrylic acid) and some associated copolymers, cements are formed which offer significant advantages as adhesive dental filling materials [4, 5]. One of these, the glass–ionomer cement has particular properties which also make it suitable for use in several non-dental applications, including surgical splinting materials [6] and foundry sand binders.

Investigations using alternative cement-forming compositions have shown that many naturally occurring silicate mineral powders will also react with aqueous polycarboxylic acid solutions to form potentially useful materials [7]. Subsequently, formulations containing well-characterized ortho- and pyrosilicate materials were studied in greater detail [8]. Their rate and extent of reaction when combined with aqueous poly(acrylic acid) solution were found to depend on the chemical composition and crystal stability of the minerals. Improvements in the rheological behaviour of cement mixtures and the mechanical properties of hardened cements were effected by reacting the minerals with an aqueous acrylic acid – itaconic acid copolymer solution. Most systems set by forming multiple polysalts, from several types of cation, to give porous products considerably weaker in compression than the analogous glass–ionomer cements. The resistance of hardened cements to hydrolytic attack varied and was dependent on the stability of the metal ion–polyacid complexes.

In continuation of these investigations, the cement-forming characteristics of certain chain, sheet and three-dimensional silicate minerals were studied and are described in the following.

2. Experimental procedure

Details of the naturally occurring chain, sheet and three-dimensional silicate minerals chosen for this investigation are given in Table I [9]. Since most of these samples were supplied in bulk form,

0022–2461/82/123575–18$04.66/0

TABLE I Silicate minerals selected for investigation

Mineral	Formula	Origin	Supplier
Chain silicates			
Wollastonite	β-$CaSiO_3$	Unknown	D
Sheet silicates			
Chlorites and serpentines			
Chrysotile	$Mg_3Si_2O_5(OH)_4$	Unknown	C
Daphnite (Bavalite)	$(Mg_{0.4}Fe^{II}_{0.7}Al_{1.5})(Si_{2.6}Al_{1.4})O_{10.2}(OH)_{7.8}$	Caradon, St Cleer, Cornwall, England	A
Thuringite	$(Mg_{2.8}Fe^{II}_{0.7}Fe^{III}_{1.4}Al_{1.2})(Si_{2.5}Al_{1.5})O_{10.8}(OH)_{7.7}$	Dona Ana County, New Mexico, USA	B
Clays			
Montmorillonite	$(\frac{1}{2}Ca, Na)_{0.33}(Al_{1.67}Mg_{0.33})Si_4O_{10}(OH)_2$	Wyoming, USA	E
Nontronite	$(\frac{1}{2}Ca, Na)_{0.33}Fe^{III}_2(Si_{3.67}Al_{0.33})O_{10}(OH)_2$	Monito, Washington, USA	B
Micas			
Biotite (Siderophyllite)	$K_2(Fe^{III}_5Al)(Si_5Al_3O_{20})(OH)_4$	St Dennis, Cornwall, England	A
Muscovite	$KAl_2(Si_3Al)O_{10}(OH)_2$	Svje, Norway	A
Three-dimensional silicates			
Zeolites			
Scolecite	$Ca(Al_2Si_3O_{10})3H_2O$	Poona, India	B
Stilbite	$(Na_2Ca)(Al_2Si_7O_{18})7H_2O$	Lagonial, Northern Ireland	A
Ultramarines			
Danalite	$Fe_4(Be_3Si_3O_{12})S$	Siker, Norway	A
Hackmanite	$Na_8(Al_6Si_6O_{24})(Cl_2, S)$	Dungannon, Ontario, Canada	B
Lazurite	$(Na, Ca)_8(Al_6Si_6O_{24})(SO_4, S)_2$	Andes of Ovalle, Chile, South America	B
Sodalite	$Na_8(Al_6Si_6O_{24})Cl$	Minas Gerais, Brazil	A
Feldspars			
Labradorite	$(Ca, Na_2)(Al_2Si_{2-3})O_8$	Isle of Skye, Scotland	A

A = RFD Parkinson, Doulting, Shepton Mallet, Somerset, England.
B = Wards Natural Science Establishment Inc, Rochester, NY, USA.
C = Cape Industries, Uxbridge, Middlesex, England.
D = Hilary Corke Minerals, Eversheds, Abinger Hammer, Surrey, England.
E = Production Chemicals (Rochdale) Ltd, Manchester, England.

they were subsequently ground to pass a 38 μm test sieve. Particle size distributions of the mineral powders were determined using a Model D Industrial Coulter Counter, with Nonidet P40 as dispersant, and Isoton II or 5% trisodium phosphate solution as supporting electrolyte. Their composition was assessed qualitatively by X-ray powder diffraction and with some samples by energy dispersive X-ray analysis. Quantitative chemical analysis of chain and sheet silicate minerals was undertaken, first by a.c. arc emission spectroscopy and then more precisely by atomic absorption spectrophotometry, for the major constituents. Three-dimensional structures were analysed by inductively coupled plasma spectroscopy, followed by a separate determination by atomic absorption spectrophotometry for specific elements which are less sensitive to this technique.

Polyacid solutions used for this study were prepared in the laboratory by previously reported procedures [3, 10] and are listed in Table II, together with some of their measured properties.

Initial stages of the cement-forming reaction involving acid attack of the mineral particles and leaching of cations into solution, were examined in a model system by suspending known amounts of each mineral powder in 0.5% $^{m}/_{m}$ aqueous poly(acrylic acid) solution for one hour. After centrifuging each mixture the aqueous layer containing extracted ions was analysed by inductively coupled plasma spectrophotometry. This procedure was repeated for three-dimensional silicate minerals reacted with 0.5% $^{m}/_{m}$ aqueous acrylic acid–itaconic acid copolymer solution. Cements were prepared by mixing the mineral powders with both 50% $^{m}/_{m}$ aqueous poly(acrylic acid) solution (PAA)

TABLE II Composition of cement-forming liquids

Polymer	Solution concentration (aqueous)	Molecular weight	Preparation procedure	Abbreviated designation
Poly(acrylic acid)	50% m/m	23 000 ($\bar{M}w$)	Free radical polymerization of acrylic acid (10)	PAA
Acrylic acid–itaconic acid copolymer	50% m/m	10 500 ($\bar{M}w$)	Free radical copolymerization of acrylic acid and itaconic acid in 2:1 mole ratio (3).	PAIA

and 50%$^{m}/_{m}$ aqueous acrylic acid-itaconic acid copolymer solution (PAIA) at the maximum attainable powder to liquid ratio, which varied between 1.0 and 2.5 g cm^{-3} depending on the reactivity of the components.

Rheological characteristics of cement pastes during setting were conveniently followed using an oscillating rheometer [11]. Infrared spectra were recorded for 24 h old cements and their parent minerals to provide information concerning the extent of reaction and the nature of reaction products. Spectra were obtained on Perkin Elmer 621 and 580B infrared spectrophotometers over a frequency range of 4000–200 cm^{-1} using samples pressed into KBr discs. In order to establish the effects of cement formation more clearly, the spectra of some cements were modified by computer subtraction of the pertinent polyacid solution spectra.

Cylindrical compressive strength specimens were prepared (in duplicate) in stainless steel moulds to British Standard specification [12], and were sealed and clamped for 24 h at 23° C. After removal from the moulds, test samples were stored for 7 days at 100% r.h. (23° C) and then immersed in either water or liquid paraffin at 23° C for a further 7 days. Control samples were also moulded and conditioned at 100% r.h. (23° C) for 14 days. All specimens were then compressed to failure in an Instron electromechanical testing machine at a cross-head speed of 1 mm min^{-1}. The solubility of hardened cement mixtures was determined (in duplicate) on moulded discs (20 mm diameter × 1.5 mm thick) formed in stainless steel split-moulds of British Standard design [12]. After setting in the moulds for 24 h at 23° C, specimens were removed and stored at 100% r.h. (23° C) for 7 days, prior to suspension in double-deionized water for an additional 7 days at 23° C. The weight of soluble extract was then measured after evaporating the water to dryness. A qualitative visual assessment of cement hydrolytic stability was also made. The microstructure of a suitably hardened, polished and gold–palladium-coated cement sample made from sodalite and PAA was examined using a Cambridge Stereoscan scanning electron microscope.

3. Results

3.1. Characterization of minerals

The compositions of the silicate minerals were determined by X-ray diffraction (XRD) and chemical analysis procedures, and are summarized in Table III. Also included in this table are qualitative results from an elemental study on certain minerals using energy dispersive X-ray analysis This study was carried out particularly for three-dimensional mineral structures, as these yielded indecisive XRD patterns. Additional evidence of mineral purity was obtained for some samples by comparing their infrared spectra (Figs 1a and b) with available reference spectra [13, 14]. Although all the chain and sheet silicate minerals were identified by XRD, many contained impurities, notably quartz. For example, the elemental analysis of wollastonite indicated a high silicon and low calcium level, consistent with the presence of SiO_2. Trace amounts of an unidentified impurity rich in Al and Mg were also observed. In the sample of chrysotile, some of the silicon was replaced by aluminium, and small quantities of magnesium were probably substituted by calcium and ferrous ions. In the chlorite group of minerals, both the daphnite (bavalite) and the thuringite samples contained silica impurities. Montmorillonite and nontronite are smectites, with layered structures capable of exhibiting cation exchange properties. The presence of iron, magnesium and sodium may result from exchange with aluminium ions. Nontronite is usually characterized by low aluminium and high iron contents [15], in agreement with the elemental analysis from this study. However, two forms of montmorillonite were identified by XRD.

Both muscovite and biotite are micas, in which a cation layer is sandwiched between layers of

TABLE III Composition of minerals

Mineral	XRD analysis	SEM analysis*	Elemental analysis (%)†								
			Si	Al	Fe	Mg	Ca	Na	K	Ti	Mn
Chain silicates											
Wollastonite	Mainly wollastonite and small amount of α-quartz and trace of unidentified impurity	Si, Ca, Al, Fe, K	27.4	1.8	0.63	1.06	19.5	0.67	1.6	0.06	0.06
Sheet silicates Chlorites and serpentines											
Chrysotile	Chrysotile only	–	17.8	0.95	3.9	22.2	0.43	0.15	0.17	0.04	0.06
Daphnite	Mixture of daphnite, α-quartz and possibly bavalite	–	31.8	5.8	10.1	0.5	0.29	0.07	1.6	0.18	0.19
Thuringite	Mainly thuringite and trace of α-quartz	–	13.0	10.4	25.0	4.3	0.29	0.06	0.08	0.24	0.38
Clays											
Montmorillonite	Mixture of two varieties of montmorillonite	–	26.7	10.3	2.7	1.37	0.79	1.6	0.33	0.12	0.012
Nontronite	Mainly nontronite and trace of unidentified impurity	–	19.4	3.1	20.9	0.5	1.29	0.06	0.17	0.04	0.006
Micas											
Biotite	Mainly biotite and trace of α-quartz and possibly potassium hydrogen silicate	–	21.8	10.8	11.8	0.5	0.14	0.22	6.7	0.3	0.19
Muscovite	Muscovite only	–	20.9	17.1	3.3	0.5	0.14	0.52	8.9	0.3	0.05
Three-dimensional silicates Zeolites											
Scolecite	No positive identification	Si, Al, Ca	20.2 (21.5)	13.0 (13.8)	0.5 –	0.12 –	9.8 (10.2)	0.1 –	0.02 –	0.05 –	–
Stilbite	No positive identification	Si, Ca, Al, Fe, Mg, Ti, Cu	19.4 (25.5)	7.6 (9.4)	5.8 –	5.1 –	5.5 (5.6)	1.0 (1.6)	0.17 –	0.53 –	–

TABLE III Continued

Mineral	XRD analysis	SEM analysis*	Elemental analysis (%)†								
			Si	Al	Fe	Mg	Ca	Na	K	Ti	Mn
Ultramarines											
Danalite	Danalite and significant amounts of α-quartz	Si, Fe, Ca, S, Al, Mg, Cu, Zn	21.4 (7.5)	2.2 –	11.8 (19.8)	1.7 –	1.7 –	0.22 –	0.16 –	0.18 –	–
Hackmanite	No positive identification	Si, Al, K, Ca	18.8 (16.8)	17.2 (16.2)	0.12 –	0.08 –	1.4 –	8.3 (18.8)	5.4 –	0.008 –	–
Lazurite	No positive identification	Si, Ca, Al, K, Fe, Cl, S	16.0 (19.0)	4.3 (18.3)	1.13 –	0.95 –	21.7 (18.1)	3.0 (10.4)	0.17 –	0.18 –	–
Sodalite	Sodalite only	Si, Cl, Al, Na	16.0 (16.2)	15.8 (15.6)	0.1 –	0.05 –	0.2 –	17.1 (17.7)	0.09 –	0.004 –	–
Feldspar											
Labradorite	Labradorite and a smectite and chabazite	Si, Ca, Al, Fe, K	19.4 –	8.1 –	7.8 –	3.8 –	6.4 –	1.7 –	0.42 –	0.8 –	

*Elements listed approximately in decreasing order of concentration.

†Analysis of chain and sheet silicates was determined by atomic absorption spectrophotometry. Three-dimensional silicates were analysed by inductively coupled plasma spectrophotometry and atomic absorption spectrophotometry (results in parentheses).

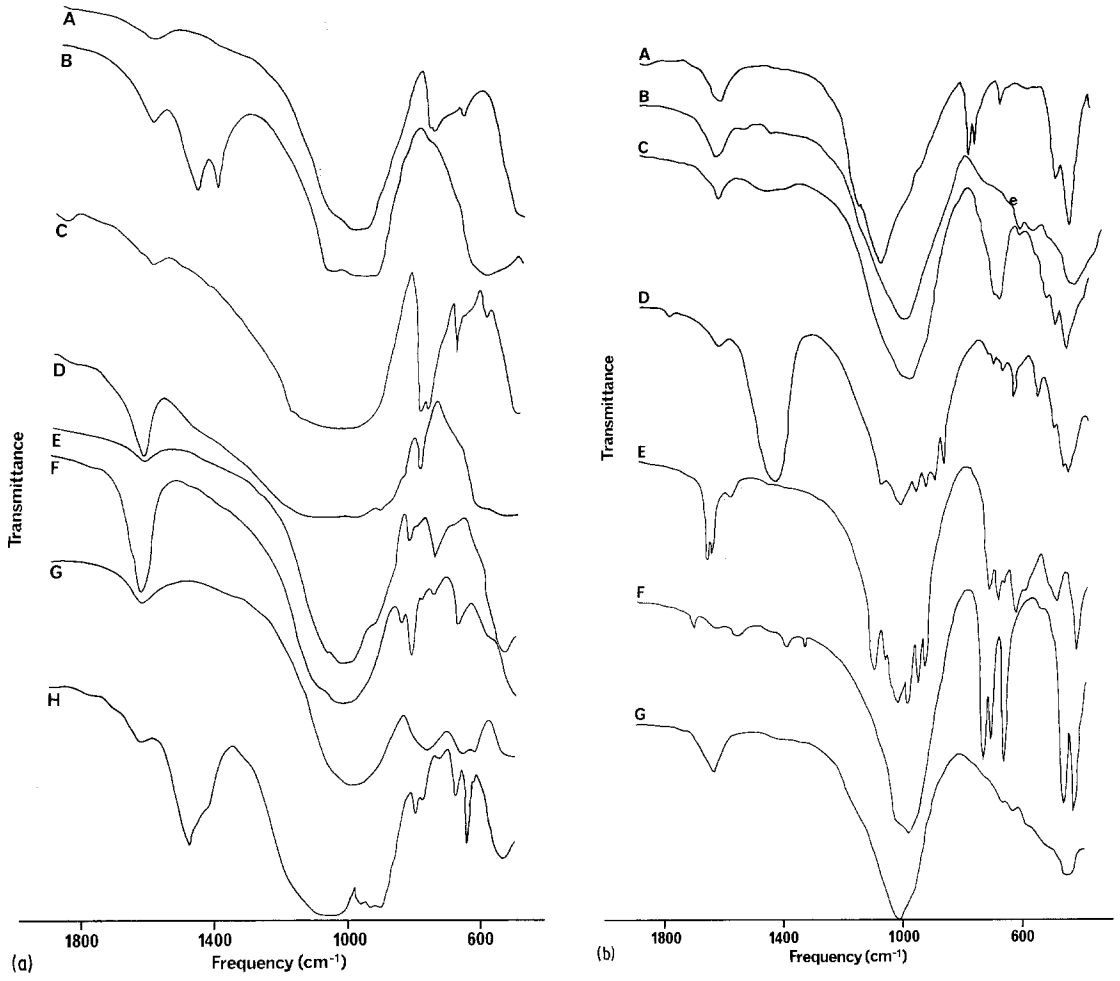

Figure 1 (a) Infrared spectra of chain and sheet silicate minerals. A, biotite; B, chrysotile; C, daphnite; D, montmorillonite; E, muscovite, F, nontronite; G, thuringite; H, wollastonite. (b) Infrared spectra of three-dimensional silicate minerals. A, danalite; B, labradorite; C, hackmanite; D, lazurite; E, scolecite; F, sodalite; G, stilbite.

linked silica and alumina tetrahedra. Biotite normally contains high magnesium and low iron contents, but the sample used in this investigation had a low level of magnesium, characteristic of a subgroup of the biotites, known as siderophyllites. The analysis and formula of muscovite agree more closely; iron is commonly found in muscovite as a replacement for aluminium.

Although the elemental analysis for the chain and sheet silicate agree fairly well with their expected compositions, it was more difficult to identify several of the three-dimensional silicates, because of their occurrence in minor quantities in feldspars. In this group there was significant evidence of iron and magnesium impurities. From chemical analysis of the zeolites, only scolecite could be classified as relatively pure. The infrared spectra of these minerals (Fig. 1b) however, showed reasonable agreement with available reference spectra [13, 14], except for an additional peak at about $1440\,cm^{-1}$ in the spectrum of lazurite, attributable to carbonate impurity.

The feldspar, labradorite, was found to contain a smectite and small amounts of chabazite as impurities; these minerals account for the high amounts of iron and magnesium found in the sample. Of the ultramarines, only sodalite was considered to be pure. In hackmanite, considerable substitution of sodium by potassium had occurred, whereas in lazurite interchange between sodium and calcium was evident. The sample of danalite contained a high concentration of silicon relative to iron caused by the presence of quartz, which was confirmed in the XRD pattern for this mineral.

Particle size distributions for all of the comminuted minerals are shown in Figs 2 and 3. Since

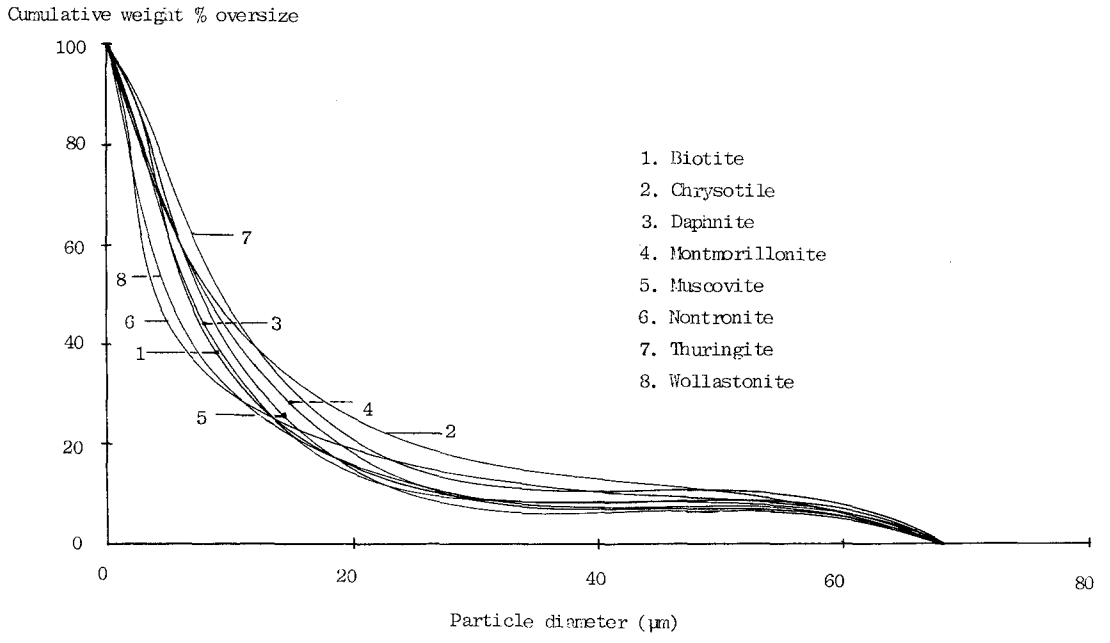

Figure 2 Particle size distributions of chain and sheet silicate minerals.

analysis with a Coulter Counter assumes a spherical particle diameter it is possible that results for chain and sheet minerals (Fig. 2) are less accurate. Consequently, values of median particle diameter are given only for those curves pertaining to three-dimensional structures, which vary between 3.4 μm (for scolecite) and 7.1 μm (for labradorite).

3.2. Cement formation

The early stages of cement formation were studied using a model system in which the mineral was subjected to attack by dilute polyacid solution and the amounts of the various elements extracted were measured. Semiquantitative results are presented in Table IV; these are expressed in terms of orders of magnitude: major (≥ 100 ppm, 100–10 ppm), minor (10–1 ppm) and trace (< 1 ppm) levels. In nearly all cases Si was extracted in major amounts; in addition, major amounts of Al, Ca and Na were also extracted from all the framework silicates. Elements leached in major amounts are of significance in terms of the cement-forming reaction and results for these are more precisely quantified, when PAA solutions were used as the extractant, in Table V. In general, the major mineral elements were extracted in the greatest concentrations, although there were exceptions. Thus, major amounts of a minor element, iron, were leached from montmorillonite into solution. For a number of minerals the presence of high concentrations of silicon, and sometimes aluminium, in the eluates was evidence of significant structural degradation of the mineral. However, danalite was anomalous, in this respect, only minor amounts of silicon being found in the PAA leachate.

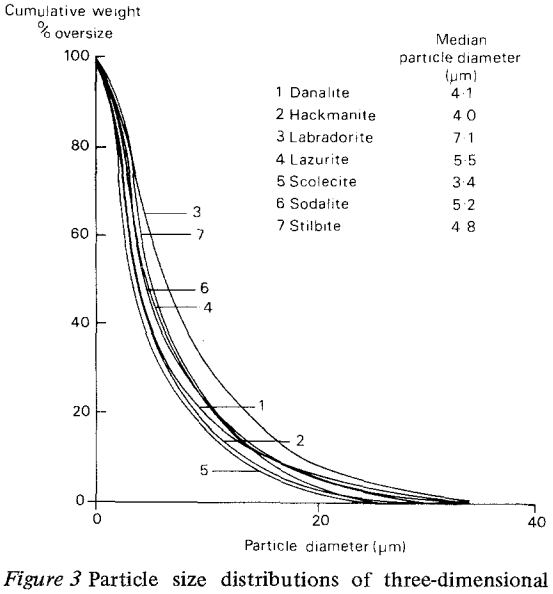

Figure 3 Particle size distributions of three-dimensional silicate minerals.

A difference spectrum (Fig. 4) obtained by subtracting the spectrum of PAIA solution from that of the scolecite–PAIA cement emphasizes mineral and polysalt absorptions which occur on cement formation. The decrease in absorption

TABLE IV Classification of mineral extract soluble ion concentration

Mineral	Major elements		Minor elements	Trace elements
	(≥ 100 ppm)	(< 100–10 ppm)	(< 10–1 ppm)	(< 1 ppm)
Chain silicates				
Wollastonite		Ca, Si	Mg, Al, Mn, Zn, K, Na	Fe, Cu, Na, Ba
Sheet silicates				
Chlorites and serpentines				
Chrysotile	Mg, Si	Ca, Fe	Al, Ni, Mn, Zn, Cu, K, Na	Ba
Daphnite	–	Al, Fe, Ca, Si, K	Mg, Mn, Na	Zn, Na, Cu, Ti, Ba
Thuringite	–	Al, Si, Fe	Mg, Zn, Ni, Mn, Ca, Cu, K, Na	Ti, Ba, Na
Clays				
Montmorillonite	Si, Fe	Mg, Ca, Na, Al	Ti, K	Zn, Mn, Cu, Ba
Nontronite	Fe	Ca, Si, Mg	Al, Na, K	Zn, Ba, Mn
Micas				
Biotite	Fe, Si, Al	Ca, Mn, Zn, Na, Mg, K	Ti, Cu	Ni, Ba
Muscovite	Si, Al, K	Fe, Zn, Ca, Na	Mg, Cu, Mn, Ti	Ba
Three-dimensional silicates				
Zeolites				
Scolecite	Si, Ca, Al	Na	Zn, Mg, Fe, K	Mn, Ni, Cu, Ti
	(Si, Al, Ca)*	(Na)	(Zn, Fe, Mg, K)	(Mn, Ni, Cu, Ti)
Stilbite	Si	Al, Ca, Mg, Na	Zn, Fe	K, Mn, Cu, Ti
	(Si, Al, Ca)	(Mg)	(Fe, Zn)	(K, Mn, Cu, Ti)
Ultramarines				
Danalite		Ca, Fe, Al	K, Mg, Zn, Si, Na	Mn, Cu, Ti
		(Fe, Ca, Si, Al, Na)	(Mg, K)	(Zn, Mn, Cu, Ti)
Hackmanite	Si, Al, Na	Ca, K	Mg, Fe	Ni, Zn, Mn, Cu, Ti
	(Si, Al, Na)	(Ca, K)	(Mg, Fe)	(Zn, Mn, Cu, Ti)
Lazurite	Ca, Si	Al, Na	Mg, Fe	Mn, Zn, Ti, Cu
	(Ca, Si)	(Al, Na)	(Mg)	(Fe, Mn, Zn, Ti, Cu)
Sodalite	Na, Si, Al	Ca, Mn	Fe, Mg, K, Zn, Cu	Ti
	(Na, Si, Al)	(Ca, Mn)	(Fe, Mg, K, Zn, Cu)	(Ti)
Feldspar				
Labradorite	Ca, Al, Si	Fe, Mg, Na	K	Mn, Zn, Cu, Ti
	(Si, Al, Ca)	(Fe, Mg, Na)	(K, Mn, Zn, Ni)	(Cu, Ti)

*Results in parentheses refer to 0.5% m/m PAIA mineral extracts.

observed for the bands at 3450 cm^{-1} and 2600 cm^{-1} indicates the loss of hydrogen-bonded and acid hydroxyl groups respectively, whereas the decrease in absorption of the band at 1720 cm^{-1} represents a reduction in the concentration of acid carbonyl groups. The increase in absorption in the bands at 1550 cm^{-1} and 1390 cm^{-1} results from the deformation of asymmetric and symmetric carboxylate stretching modes in the set cement. These changes can be seen in the infrared spectra of selected mineral cements (Fig. 5).

The setting characteristics of mineral–cement pastes, obtained from oscillating rheometer traces, are summarized in Table VI, in terms of working times (defined as 90% of the initial amplitude value) and setting times (taken as the time to reach a limiting amplitude). A description of cement consistency on setting is also included. Because of the extremely rapid reaction rate of some minerals towards polyacid solutions, in many of the compositions, the powder to liquid ratio was lowered to facilitate cement manipulation. This was most necessary with mixtures made from three-dimensional silicate minerals, in particular with scolecite and sodalite. Several of the mixtures were considered to have set, even though they failed to completely harden, and retained some degree of plasticity or rubberyness. Differences in setting behaviour are also demonstrated by selected rheometric traces shown in Fig. 6. For example the lazurite–PAA cement paste (Fig. 6a)

TABLE V Major quantities of mineral extracts in PAA solution ($\mu g\ ml^{-1}$)

Mineral	Al	Ca	Fe	K	Mg	Mn	Na	Si	Zn
Chain silicates									
Wollastonite		> 71						41.2	
Sheet silicates									
Biotite	117	32.2	270	96	11.0	15.8	13	161.8	13.1
Chrysotile		> 71	27.3		> 290			111.8	
Daphnite	32	41.9	50.6	11				20.6	
Montmorillonite	65	34.2	128.5		62.8		52	93.2	
Muscovite	153	13.9	44.5	104			11	132.3	40.4
Nontronite		> 71	127.7		22.8			26.5	
Thuringite	12		10.3					20.6	
Three-dimensional silicates									
Danalite	13	22	20.9						
Hackmanite	326	73		69.6			143	350	
Labradorite	102	106	23.8		19.3		40	100	
Lazurite	33	590					70	122	
Scolecite	121	148					22	260	
Sodalite	329	19			10.7		240	346	
Stilbite	98.7	79			17.2		34	114	

clearly showed three stages during setting. During the first three minutes after the start of mixing, the amplitude of the trace is almost constant, indicating that the viscosity of the cement paste did not change. This is followed by a period where the amplitude decreased rapidly as the composition thickened. A final stage is reached where the amplitude was small and constant and the cement was considered to have set. In contrast, however, the rheogram for the labradorite–PAA cement paste (Fig. 6b) shows an immediate and sharp decline in amplitude, then a protracted final setting stage. A rheogram for the hackmanite – PAIA cement (Fig. 6c) has similar features except that the ultimate setting is more rapid and closely defined.

Wherever possible compressive strengths of mineral-cements have been listed in Table VI. Highest values were obtained for compositions containing PAA mixed with labradorite, hackmanite and scolecite, although in several samples cement strength was clearly affected by their hydrolytic instability. In some cases water absorption caused softening, swelling and cracking of the samples. For example, labradorite formed a strong cement with PAA, when stored at 100% r.h., but weakened considerably when conditioned in water. The high solubility values measured for many of the cements (Table VI), also reflect their susceptibility to aqueous attack.

The composite microstructure represented in Fig. 7 is typical of hardened mineral cements made from an excess of mineral powder in polyacid liquid, and shows unreacted mineral powder

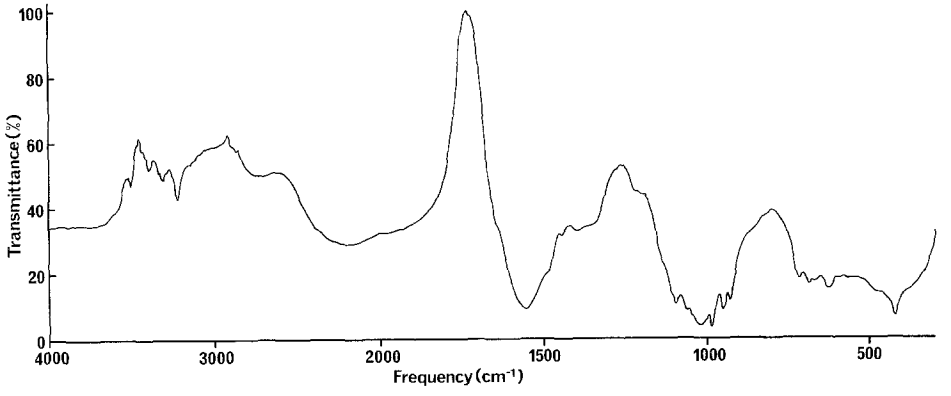

Figure 4 Infrared difference spectrum between scolecite–PAIA cement and PAIA solution.

TABLE VI Physical properties of mineral cements

Mineral	Powder[a]–liquid ratio ($g\,cm^{-3}$)	Working[b] time at 23° C (min)	Setting time[c] at 23° C (min)	Compressive strength (MPa)		Cement description on setting	Solubility[d] (wt %)	Hydrolytic stability
				14 days at 100% r.h. (23° C)	7 days at 100% r.h. (23° C) + 7 days in water (23° C)			
Chain silicates								
Wollastonite	1.0	1.7	13.7	–	22[e]	Hard, brittle	7	Softened
	(1.5)	(2.0)	(13)	(18)	(3.4)	(Hard, brittle)	(3.7)	
Sheet silicates								
Biotite	1.0	1.95	Did not set	–	8[e]	Plastic	20	Unstable
	(1.5)	(2.5)	(136)			(hard, brittle)		(unstable)
Chrysotile	1.5	5.9	54	–	–	Soft	–	Unstable
	(2.0)	(7.5)	(37)			(hard, brittle)		(unstable)
Daphnite	1.5	2.9	86.5	–	–	Hard, tough	2	Dimensionally
	(2.0)	(4.0)	(34)			(crumbly solid)	(1.8)	unstable
Montmorillonite	1.0	2.0	Did not set	–	–	Soft, crumbly	20	Unstable
	(1.0)	(< 1.5)	(35)			(hard, brittle)		(unstable)
Muscovite	1.0	1.45	72	2.5	19[e]	Soft, crumbly	13	Softened
	(1.5)	(2.0)	(20)			(tough, solid)		(softened)
Nontronite	1.0	1.6	137	1	1[e]	Hard, brittle	24	Softened
	(1.5)	(< 2.0)	(18)			(hard, brittle)		(unstable)
Thuringite	1.5	1.8	29	28	35	Hard, brittle	1	Stable
	(2.0)	(4.0)	(30)	(19)	(16)	(hard, brittle)	(1.3)	(stable)
Three-dimensional silicates								
Danalite	2.0	1.2	19	–	–	Rubbery	7.7[f]	Softened
Hackmanite	1.0	1.3	13.4	89	37	Hard solid	2.4	Stable
	(1.0)	(< 1.0)	(14)	(37)	(28)		(2.4)	(stable)
Labradorite	1.0	1.2	59	134	1.7	Rubbery	3.6	Slightly
	(1.5)	(< 1.0)	(18)	(21)	(10)		(6.5)	unstable
Lazurite	1.0	2.6	20[g]	–	–	Rubbery	6.4	Softened
	(1.0)	(7.2)	(35)	(6.5)	(4.3)		(2.9)	

TABLE VI Continued

Mineral	Powder[a]–liquid ratio ($g\,cm^{-3}$)	Working[b] time at 23° C (min)	Setting time[c] at 23° C (min)	Compressive strength (MPa)		Cement description on setting	Solubility[d] (wt %)	Hydrolytic stability
				14 days at 100% r.h. (23° C)	7 days at 100% r.h. (23° C) + 7 days in water (23° C)			
Scolecite	0.5 (1.0)	1.2 (1.0)	– (20)	160 (27)	30 (29)	Hard, set via rubbery stage (hard)	1.35 (1.33)	Slight instability
Sodalite	0.5 (1.0)	1.1 (< 1.0)	25.2 (32)	– (16)	– (11)	Hard, set via rubbery stage (hard)	4.3 (2.0)	Some instability
Stilbite	1.5 (1.5)	1.5 (4.0)	30 (50)	23 (8)	7 (1.6)	Hard, set via rubbery stage (hard)	2.6 (4.1)	Some instability

Results in parentheses refer to cements made using PAIA solution. All other results are for mineral–PAA mixtures.

[a] Cements were mixed at maximum possible powder to liquid ratio.

[b] Determined from 90% of initial amplitude on the rheometer trace.

[c] Results obtained from rheometric trace.

[d] Determined after 24 h sealed storage + 7 days at 100% r.h. (23° C) + 7 days in water at 23° C.

[e] Samples stored for 7 days at 100% r.h. (23° C) + 7 days in liquid paraffin at 23° C.

[f] At P/L = 1.5 $g\,cm^{-3}$.

[g] H_2S evolved on mixing.

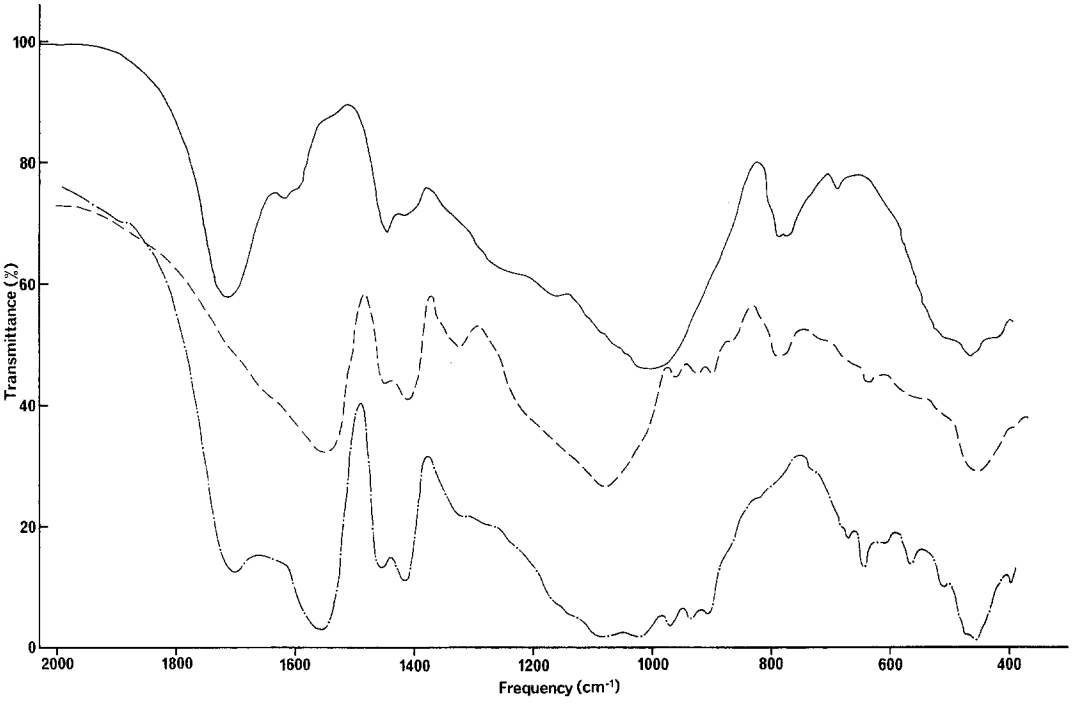

Figure 5 Infrared spectra of mineral cements. (a) Biotite–PAA cement ——; (b) wollastonite–PAA cement – – – –; (c) lazurite–PAA cement –.–.–.–.

particles bound in surrounding polymeric-gel matrix. The cracks observed at the particle-matrix interface result from the shrinkage of the matrix under the high vacuum conditions employed in the scanning electron microscope.

4. Discussion

4.1. Acid decomposition of minerals

The susceptibility of silicate minerals to acid attack may be explained by reference to their elemental composition and the nature of their molecular structures. Murata [16, 17] in an extensive survey of silicate minerals which are vulnerable to acid attack, concluded that three-dimensional silicates, such as sodalite, lazurite and scolecite, in which the ratio of Al:Si ions in the network is at least 2:3, are usually completely decomposed by acids, with the formation of silica gel. Minerals which are characterized by silicon–oxygen structures of larger dimensions, such as $(SiO_3)_n^{2n-}$ single chains, $(SiO_{11})_n^{6n-}$ double chains, or $(SiO_5)_n^{2n-}$ sheets, with little or no isomorphous replacement of Fe^{3+} or Al^{3+} for Si^{4+} do not usually gelatinize in the presence of acids, but only partially decompose to separate insoluble silica. Such behaviour has been found to occur with montmorillonite and biotite. In thuringite and nontronite however, there is significant iso-morphous substitution of Si^{4+} by Al^{3+} and Fe^{3+} in the sheet structure, rendering the network more protophilic and susceptible to acid attack; following decomposition therefore, silica gel is formed. A precise understanding of the acid decomposition of many silicate minerals is further complicated by the probable shielding effect created by giant silicate anions found in chain, sheet and three-dimensional structures. Clearly minerals with open structures, found with some chain-silicates such as wollastonite, and also in the zeolites, will be more rapidly penetrated by protons. There is evidence to suggest the ionic potential of metal cations bound in the mineral network, may also be a determining factor, since strongly polarizing ions such as Fe^{3+} and Mn^{3+} can increase the bonding energy and chemical stability of the mineral lattice [18]. Chrysotile has a sheet structure, but unlike montmorillonite for example, it does not form planar sheets, but curved layers of silica and brucite ($Mg(OH)_2$) combined in the form of a concentric cylinder [19]. When attacked by acids it is completely stripped of the outer brucite layer leaving a silica skeleton.

4.2. The setting reaction

The setting of mineral cements probably occurs in a number of overlapping stages consisting of acid

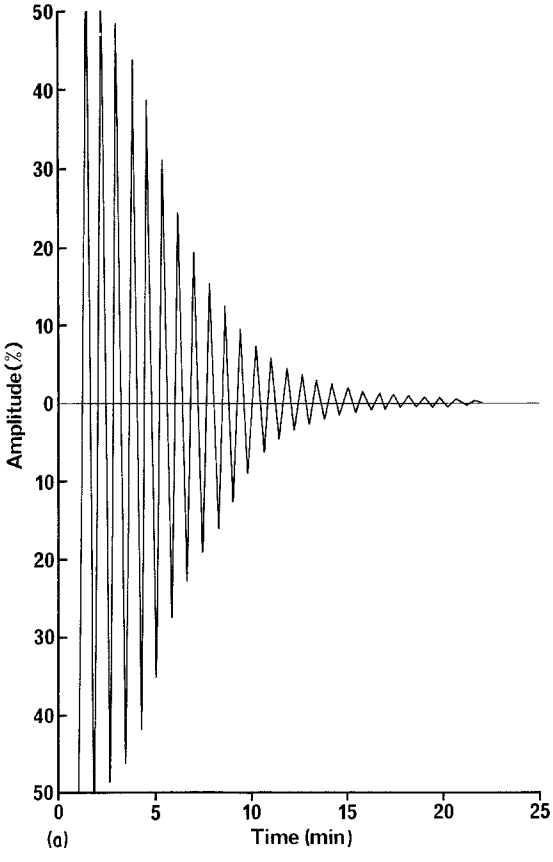

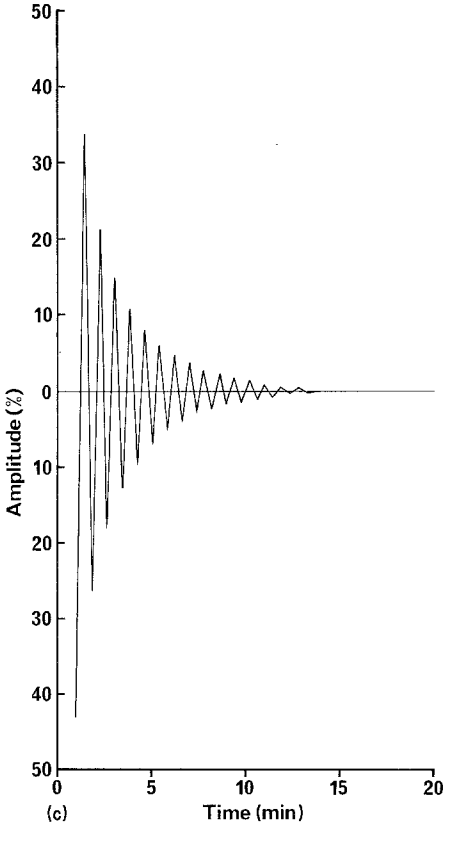

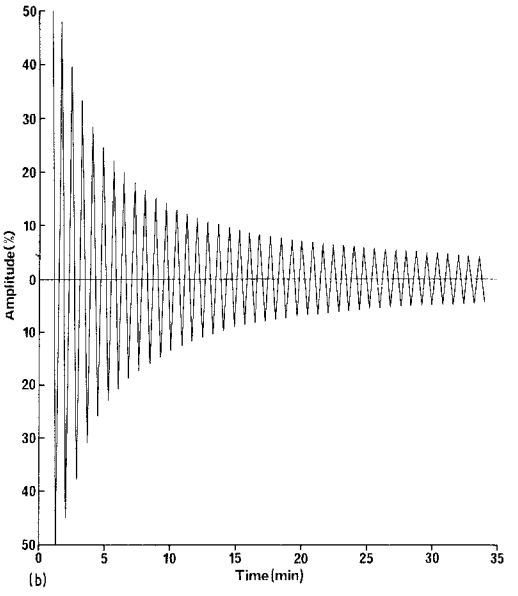

Figure 6 Oscillating rheometer traces for (a) Lazurite–PAA cement; (b) labradorite–PAA cement; (c) hackmanite–PAIA cement.

attack and ion-leaching from the mineral powder, initial precipitation and gelation of the polyacid as ion-binding ensues, and ultimately longer-term hydration reactions, which cause the hardened cement to progressively develop in strength [20]. The precipitation phase of the reaction, involving the formation of polysalts is confirmed by the infrared spectra of hardened cements (Table VII and Figs 4 and 5). The position of the peaks arising from the asymmetric carboxylate stretching modes at 1530–1600 cm^{-1} reflects the nature of metal-ion association with the polyacid [21]. Peaks at about 1540 cm^{-1} are observed when calcium, magnesium, zinc or sodium ions bind ionically to polyacrylate, whereas aluminium polyacrylate shows an additional peak at about 1600 cm^{-1} because of covalent binding. The infrared spectroscopic data (Table VII) suggest that several of the compositions, in particular those made from daphnite, muscovite, nontronite and thuringite, contain both coordinated and ionically bonded metal salts in their matrix. In each case, the precise nature of the ions involved in the complex is subject to speculation, but reference to Table IV does indicate that major amounts of Al and Fe are released into dilute acid solution from all but nontronite, which contains large amounts of soluble Fe but not Al. This suggests that either or both of these elements may be covalently bound in the polysalt matrix.

TABLE VII Salt formation in mineral–polyacid cements

Mineral	Reaction with PAA					Reaction with PAIA				
	Acid carbonyl absorption (cm^{-1})	Acid carboxylate absorptions (cm^{-1})			Conclusion	Acid carbonyl absorption (cm^{-1})	Acid carboxylate absorptions (cm^{-1})			Conclusion
Chain silicates										
Wollastonite	1700(sh)		1550(b)	1410	Little acid remaining; ionic salt formed	1700(sh)		1560(b)	1400	Little acid remaining; ionic salt formed
Sheet silicates										
Biotite	1710		1540	1410	Very little reaction; ionic salt formed	1720	1595	1545	1410	Very little reaction; some ionic salt formed
Chrysotile	1710		1550(b)	1415	Some acid left; ionic salt formed	1710		1560(b)	1410	Some acid left; ionic salt formed
Daphnite	1710	1590	1540	1415	Some acid left; ionic and possibly coordinated salt formed	1715	1595	1545	1400	Acid remaining; ionic and coordinated salt formed
Montmorillonite	–		–		–	1715		1530	1410	Very little reaction; mainly acid present
Muscovite	1715	1590	1540	1400	Some reaction; ionic and possibly coordinated salt formed	1720	1600	1540	1400	Acid remaining; ionic and coordinated salt formed
Nontronite	1715	1590	1540	1420	Some reaction; ionic and possibly coordinated salt formed	1710	1590	1540	1410	Acid remaining; ionic and coordinated salt formed
Thuringite	1705	1585	1550	1415	Some acid remaining; ionic and coordinated salt formed	1710	1585	1550	1410	Acid remaining; ionic and coordinated salt formed
Three-dimensional silicates										
Danalite	1715	1595		1420	Acid remaining; coordinated salt formed	1720	1600(sh)		1420 1405	Acid remaining; coordinated salt formed
Hackmanite	1720		1560(sh)	1410	Unreacted acid present; ionic salt formed	1720		1560(sh)	1405	Unreacted acid remaining; ionic salt formed

TABLE VII Continued

Mineral	Reaction with PAA				Reaction with PAIA			
	Acid carbonyl absorption (cm^{-1})	Acid carboxylate absorptions (cm^{-1})		Conclusion	Acid carbonyl absorption (cm^{-1})	Acid carboxylate absorptions (cm^{-1})		Conclusion
Labradorite	1715	1600(sh) 1560(sh)	1410	Unreacted acid present; ionic salt formed	1715	1560(sh)	1410	Free acid present; ionic salt formed
Lazurite	1700	1550	1415	Some free acid remaining; ionic salt formed	1700	1560	1480	Some free acid remaining; ionic salt formed
Scolecite	1715	1550(sh)	1405	Free acid present; ionic salt formed	1710	1560	1405	Less free acid than with PAA; ionic salt formed
Sodalite	1715	1560	1405	Free acid remaining; ionic salt formed	1705	1565	1400	Less free acid than with PAA; ionic salt formed
Stilbite	1710	1560	1410	Free acid present; ionic salt formed	1710	1560(sh)	1405	Free acid remaining; ionic salt formed

(sh) = shoulder; (b) = broad.

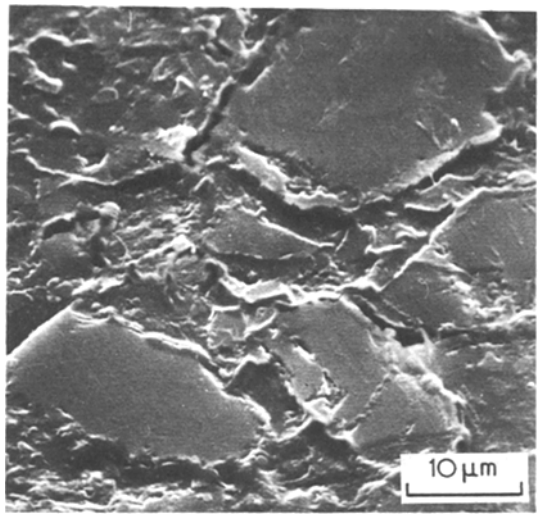

Figure 7 Electron micrograph of the sodalite–PAA cement.

However, other reactive minerals, such as hackmanite and sodalite, also contain comparable concentrations of aluminium in their acid extracts, without signs of coordinated salt formation in their infrared spectra. In these compositions, it would appear that the ionic form of aluminium–polyacrylate may predominate over the covalent form. There is little effect on cement gel structure of using PAIA in place of PAA solution, except that many infrared salt absorptions tended towards a higher frequency with the copolymer solution, indicative of increasing covalency in the metal ion–polyacid bond.

The magnitude of the acid carbonyl peak (1700–1720 cm^{-1}) relative to the intensity of the asymmetric carboxylate peak is a measure of the extent of neutralization. Applying this criterion to the spectra of one-day old cements gives an approximate order of decreasing degree of reaction for chain and sheet silicates as: wollastonite > chrysotile > thuringite > daphnite > muscovite, nontronite > montmorillonite > biotite. For three-dimensional silicate cements the extent of salt formation varies according to the following sequence: lazurite > danalite > hackmanite, stilbite, sodalite, labradorite > scolecite.

4.3. Rheology of cement pastes

The rheology of setting mineral–PAA cement pastes passes through a number of characteristic stages. Most pastes remain workable for only a short time (1–2 min), then become unworkable for a longer and more variable period before setting (Table VI). In general three-dimensional minerals react more vigorously with polyacid solutions than do the chain and sheet minerals, which were the subject of a previous study [8]. Again, the moderating effect on reactivity, of substituting PAIA for PAA, was observed and frequently enabled cement pastes to be mixed at higher powder to liquid ratios and in some systems gave a reduction in the ultimate setting time. The improvements in manipulative characteristics are in part due to the lower viscosity of the PAIA liquid, which results in greater mobility of the cement paste during mixing [22]. The physical form of the set cements, which vary from being soft or rubbery to hard and brittle (Table VI), is often predictable from their rheometer traces. For example, the rapid decay to zero amplitude in the rheograms for hackmanite–PAIA and lazurite–PAA cement mixtures demonstrates that these compositions set to a rigid mass soon after the commencement of mixing (Fig. 6), whereas the trace for labradorite–PAA shows that a rubbery product is formed on setting, characterized by a high limiting amplitude. The inability of biotite and montmorillonite to set when mixed with PAA solution is most probably a reflection of the low degree of reaction in these compositions. Chrysotile however, also yields a soft cement, but reacts extensively with PAA. This observation may be explained in terms of the low crosslinking efficiency of the principal salt-forming cation, Mg^{2+}, as discussed in an earlier communication relating to olivine–PAA cement mixtures [8]. Many of the three-dimensional silicate–polyacid mixtures are characterized by their tendency to set rapidly to rubbery products, which then slowly increase in rigidity over a period of 24 h. In these systems the initial setting reaction may involve weak binding by divalent cations separated from the polyacrylate chain by a primary hydration layer and held only by ionic forces [23]. In the later stages of the reaction this water may be displaced by trivalent cations such as Al^{3+}, to form either contact ion-pairs or covalently bound salts, thereby increasing the rigidity of the cement. Such a phenomenon has been observed in glass–ionomer cements, where a progressive reduction in plasticity occurs as Al^{3+} ions crosslink the polyanion chains [24].

4.4. Mechanical properties and hydrolytic stability

Compressive strengths of hardened cements made

from PAA combined with labradorite, hackmanite and scolecite, then stored for 14 days at 100% r.h. (23° C) (Table VI), compare favourably with the value of 114 MPa obtained for a glass–ionomer cement mixed at $1:1\,g\,cm^{-3}$ powder to liquid ratio, and conditioned in a similar way before testing [25]. The strength of hardened mineral cements is significantly affected by inherent porosity, which is usually most evident in compositions containing carbonate impurity, as in the cement made from lazurite. Evolution of H_2S from lazurite probably weakens this cement further. Compressive strengths of cements are also critically dependent on their resistance to aqueous attack. With most samples immersion in water causes significant reductions in mechanical properties, probably by hydrolysis of crosslinks between the chains, causing either total structural breakdown of the composite, or softening due to the plasticizing action of the water. Wollastonite–, lazurite– and sodalite–PAIA cements are stronger than the corresponding PAA cements, probably due to their greater hydrolytic stability. However, the weakening effect caused by using PAIA solution in place of PAA, in cements made from labradorite, hackmanite and scolecite, is more difficult to explain, particularly as the copolymer solution permitted formulation at the same or increased powder to liquid ratios.

The nature of the cations present in the polysalt matrix has a profound effect on the hydrolytic stability of set cements. Minerals which contain large amounts of soluble Ca^{2+} have a tendency to form cements which soften in water, as exemplified by compositions made from wollastonite and lazurite, whereas the instability of chrysotile–PAA cements may be accounted for by the greater susceptibility to hydrolysis of the magnesium polyacrylate matrix. The formation of aluminium polyacrylate however, would seem to confer some degree of hydrolytic stability on mineral cements. For example, thuringite and hackmanite both form stable cements when mixed with PAA, most probably due to the significant amounts of Al^{3+} leached from these minerals (Table V). Several compositions show signs of slight instability when immersed in water. Cements containing labradorite, scolecite and stilbite fall into this category. Although these minerals possess large amounts of soluble Al^{3+}, they also release into acid solution equivalent quantities of Ca^{2+}, which would be expected to weaken the resistance of the resulting gel matrix towards hydrolytic attack. Similarly the cement matrix formed from sodalite and PAA may be more easily disrupted by the presence of unstable sodium polyacrylate.

5. Conclusions

The early stages of the cement-forming reaction which occurs when chain, sheet or three-dimensional silicate minerals are mixed with aqueous polycarboxylic acid solutions, involve acid-decomposition of the mineral powder and release of compositional elements into solution. Mineral solubility is enhanced in open structures, particularly those which exhibit isomorphous substituion of Si^{4+} by Al^{3+} or Fe^{3+}. Soluble metal ions subsequently combine with negatively charged polymer chains to form polysalts, causing gelation and solidification of the cement mixture. The nature of ion-binding is complex and varies from largely covalent association, with ions such as Al^{3+} and Fe^{3+}, to ionic attraction with Mg^{2+}, Ca^{2+} and Na^{+}. In several mineral cements both forms of bonding coexist.

Many cement pastes have very short working times and set rapidly to a hard brittle mass. Other systems however, form soft or rubbery products, particularly when the degree of reaction is low or the matrix is weakly crosslinked, e.g. magnesium polyacrylate. Some formulations made with three-dimensional silicates immediately set to a rubbery material, which slowly hardens on ageing, indicative of a time-dependent increase in the number and strength of matrix crosslinks. With most cement mixtures, manipulative properties are significantly improved using PAIA solution as an alternative to PAA.

Minerals, such as hackmanite and thuringite which release large amounts of Al^{3+} into solution, form hydrolytically stable cements with PAA, due to the low solubility of aluminium polyacrylate. Cements which contain calcium polyacrylate in their matrix, however, frequently soften when immersed in water, whereas the presence of sodium and magnesium polysalts causes even greater instability. The compressive strength of mineral cements is frequently dependent on their resistance to hydrolysis. For example some minerals, such as labradorite and scolecite, form cements with PAA, which are as strong as analogous glass–ionomer dental cements when stored at 100% r.h., but weaken considerably when placed in water.

Acknowledgements

The authors thank Dr J. Arnold, Mr S. Wyles and Mr K. Hassal for elemental analyses, and Mrs P. King and Mr P. Bottomley for determining infra-red spectra of the minerals and their cements. Mr B. R. Young (Institute of Geological Sciences) is thanked for identification of some three-dimensional silicates.

References

1. A. D. WILSON, *Brit. Polym. J.* **6** (1974) 165.
2. J. ELLIOTT, L. HOLLIDAY and P. R. HORNSBY, *ibid* 7 (1975) 297.
3. A. D. WILSON and S. CRISP, *ibid* 7 (1975) 279.
4. D. C. SMITH, *Brit. Dent. J.* **125** (1968) 381.
5. A. D. WILSON and J. W. McLEAN, *Aust. Dent. J.* **22** (1977) 31.
6. W. D. POTTER *et al.*, US Patent No. 4043327 (1977).
7. S. CRISP, A. D. WILSON, J. H. ELLIOTT and P. R. HORNSBY, *J. Appl. Chem. Biotechnol.* **27** (1977) 369.
8. S. CRISP, S. MERSON, A. D. WILSON, J. H. ELLIOTT and P. R. HORNSBY, *J. Mater. Sci.* **14** (1979) 2941.
9. E. S. DANA, "A Textbook of Mineralogy", revised by W. E. Ford, 4th edn (John Wiley, New York and London, 1966).
10. D. C. SMITH, British Patent No. 1139430 (1969).
11. C. G. PLANT, I. H. JONES and H. J. WILSON, *Brit. Dent. J.* **133** (1972) 21.
12. British Standards Specifications for Dental Glass Ionomer Cement BS 6039 (1981).
13. H. H. W. MOENKE, in "The Infra-red Spectra of Minerals", edited by V. C. Farmer (Mineralogical Society, London, 1974).
14. H. W. VAN DE MAREL and H. BEUTELSPACHER, "Atlas of Infra-red Spectroscopy of Clay Minerals and their Admixtures" (Elsevier, London, 1976).
15. W. A. DEER, R. A. HOWIE and J. ZUSSMAN, "Rock-Forming Minerals", (Longman, London, 1974).
16. K. J. MURATA, *American Mineralogist* **28** (1943) 545.
17. *Idem, Geological Survey Bulletin* **950** (1942) 25.
18. H. MASE, *J. Chem. Soc. Japan* **34** (1961) 214.
19. A. A. HODGSON, "Fibrous Silicates", Royal Institute of Chemistry Lecture Series No. 4 (1965).
20. A. D. WILSON, *Chem. Soc. Rev.* 7 (1978) 265.
21. S. CRISP, H. J. PROSSER and A. D. WILSON, *J. Mater. Sci.* **11** (1976) 36.
22. S. CRISP, A. J. FERNER, B. G. LEWIS and A. D. WILSON, *J. Dentistry* **3** (1975) 125.
23. A. IKEGAMI and N. IMAI, *J. Polymer Sci.* **56** (1962) 133.
24. S. CRISP, M. A. PRINGUER, D. WARDLEWORTH and A. D. WILSON, *J. Dent. Res.* **53** (1974) 1414.
25. P. R. HORNSBY, PhD Thesis, Brunel University (1977).

Received 22 April
and accepted 24 May 1982